Electrochemical and Solid-State Letters, **10** (4) A111-A114 (2007)
1099-0062/2007/10(4)/A111/4/$20.00 © The Electrochemical Society

Atomic Layer Structure of Vanadium Oxide Nanotubes Grown on Nanourchin Structures

C. O'Dwyer,[a,z] V. Lavayen,[a,b] S. B. Newcomb,[c] E. Benavente,[d] M. A. Santa Ana,[b] G. González,[b] and C. M. Sotomayor Torres[a]

[a]*Tyndall National Institute, University College Cork, Cork, Ireland*
[b]*Department of Chemistry, Faculty of Science, Universidad de Chile, Santiago, Chile*
[c]*Glebe Scientific Limited, Newport, County Tipperary, Ireland*
[d]*Department of Chemistry, Universidad Tecnológica Metropolitana, Santiago, Chile*

We report the detailed characterization of high quality vanadium oxide (VO_x) nanotubes (NTs) and highlight the zipping of adjacent vanadate layers in such NTs formed on remarkable nanourchin structures. These nanostructures consist of high-density spherical radial arrays of NTs. The results evidence vanadate NTs with unprecedented uniformity and evidences the first report of vanadate atomic layer zipping. The NTs are ~2 μm in length with inner diameters of 20–30 nm. The tube walls comprise scrolled triplet-layers of vanadate intercalated with organic surfactant. Such high-volume structures might be useful as open-access electrolyte scaffolds for lithium insertion-based charge storage devices.
 [DOI: 10.1149/1.2436645]

Manuscript submitted October 9, 2006; revised manuscript received November 30, 2006.
Available electronically February 2, 2007.

Direct architecture of complex nanostructures is highly desirable and still remains a challenge in area of materials science.[1,2] Due to their size and shape dependent electronic and optical properties, significant effort has been made to control morphologies of transition metal oxide nanostructures and to organize them into complicated three-dimensional structures using templates.[3,4]

Lithium insertion into vanadium oxide thin films and other products has been investigated extensively, particularly from the point of view of their use as electrode materials in rechargeable lithium batteries.[5-8] Promising results have been reported for amorphous and low-crystallinity materials such as V_2O_5 xerogels and aerogels,[7] as well as for vanadate $Li_{x+1}V_3O_8$.[9] Amine-embedded vanadate layers can be readily exchanged with various metal cations such as alkaline, alkaline earth, and transition metal ions, with preservation of the tubular morphology.[10] Such properties allow for the realization of tailor-made functional materials. Furthermore, successful lithium ion insertion into tubular vanadates has only recently been achieved; the next stage is the synthesis of more complex structures with greater volume for lithium ion insertion. Accurate characterization of the nanostructure, however, is essential in realizing new nanostructures than can accommodate interatomic layer cations.

By far, most of the electron microscopical investigations of vanadate nanotubes have been performed with the electron beam perpendicular to the tube axis.[11] A longitudinal projection would allow for an investigation of the tube morphology and wall growth characteristics. Employing cross-sectional analysis allows us to discriminate between scrolls of layers and cylindrical layer arrangements during nanotube formation.[12] This Letter reports on the structural characteristics of vanadium oxide nanotubes (NTs) observed to grow from a spherical, hollow-centered structure known as nanourchin,[13] successfully synthesized by a simple chemical route, and accurately classifies both the vanadate atomic layer characteristics, defects, and adjacent layer zipping between adjacent tubes. The findings are promising for high-volume lithium insertion and the structures could potentially be employed as open-access electrolyte scaffolds.

Experimental

A solution of 10^{-3} mol of hexadecylamine (HDA) in 10 mL of pure ethanol, previously degassed by repetitive freeze-thaw cycling in an argon vacuum, was mixed with 2×10^{-3} mol vanadium (V) triisopropoxide (VOTPP). The yellow solution, obtained after vigorous stirring for 1 h, was then hydrolized by adding 15 mL of doubly deionized pure water, yielding an orange suspension after stirring for 24 h. The hydrothermal treatment of the orange suspension was performed in a Teflon lined autoclave at 180°C. From the resulting dark suspension a dark solid was separated, washed with pure ethanol and water, dried under vacuum (10^{-3} mmHg) for 48 h at room temperature, and stored under argon atmosphere. The final product has the composition $V_2O_5(HDA)_{0.83}\cdot 1.8H_2O$. Analysis: Exp. (calculated for $C_{13.28}H_{32.65}N_{0.83}O_{6.8}V_2$), C:39.06(38.32); H:8.05(7.89); N:2.56(2.79).

X-ray powder diffraction characterization was performed using a Siemens D5000 diffractometer (Cu Kα, λ = 1.5418 Å, operation voltage = 40 kV, current = 30 mA). Field-emission scanning electron microscopy (FESEM) was performed with a JEOL JSM-6700F. Electron transparent specimens were prepared by ion-milling techniques and placed on a holey carbon support. Transmission electron microscopy (TEM) and electron diffraction (ED) were conducted using a JEOL 2000FX operating at 200 kV and a Philips CM300 FEGTEM operating at 300 kV.

Results and Discussion

An example of an individual nanourchin is shown in the FESEM micrograph in Fig. 1A. High-resolution transmission electron microscopy (HRTEM) investigations have unveiled the detailed structure of these NTs. A typical TEM image of the NTs is shown in Fig. 1B. The NTs are most often composed of an even number of parallel vanadate atomic layers in its distorted octahedral γ–V^{5+} conformation.[14,15] The longest NTs are measured to be several micrometers in length with overall diameters of 80–100 nm and hollow centers typically measured to be 20–30 nm.[12,13,16] The majority (>90%) of NTs are observed to be open-ended and appear to be rolled up as evidenced by the diffraction contrast variation at the tips, confirming the mechanism proposed by Chen et al.[16]

The micrograph (Fig. 1B) highlights the uniform tubular nature of the nanourchin tubes; a constant 20 nm diameter hollow center extends to the tip of each NT that is flanked by equal thickness tube walls. The sidewalls of the tube are composed of regularly spaced lattice planes. The only defects observed in these NTs are lattice-plane dislocations.

For the purpose of investigating the longitudinal shape and structure of the nanotubes, the TEM images (Fig. 2) show that the tube walls consist of alternate layers that appear with bright and dark contrast. In particular, TEM images in the longitudinal projection clearly reveal that the NTs have open ends, seen at **T** and **L** in Fig. 2A and there is a clear tendency for overlap in some areas, such as at **S**, which has never been previously observed. In the majority of TEM observations of these tubes, we observe the central scroll at **T** to be closed. This unique observation explains the long-range uni-

[z] E-mail: codwyer@tyndall.ie

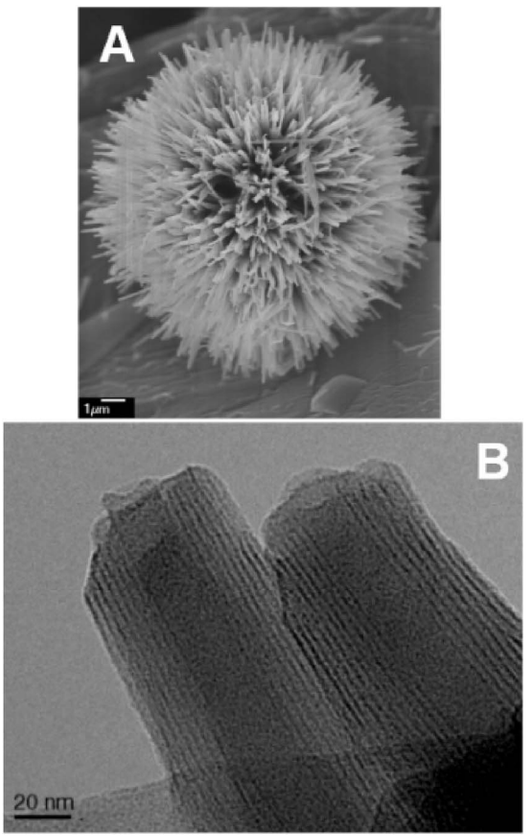

Figure 1. (A) FESEM image of an individual nanourchin, (B) high-resolution bright field TEM images of fully developed nanotube tips in the nanourchin showing evidence for vanadate layer rolling.

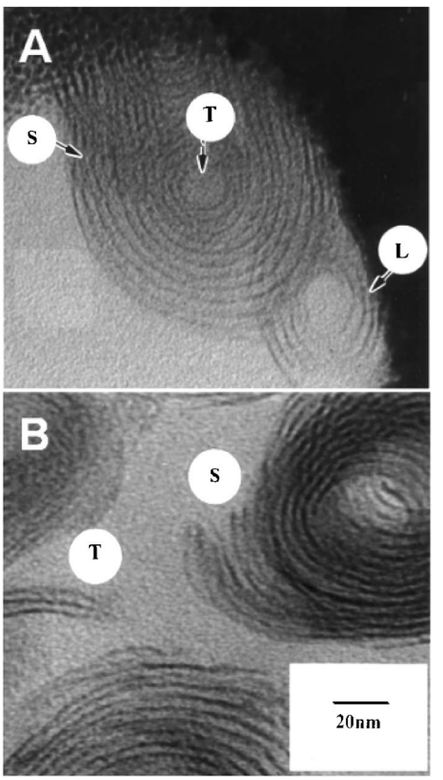

Figure 2. High-resolution bright field TEM image along (A) direct and (B) angled longitudinal directions showing the nanotube cross-sections.

formity of the inner hollow diameter. Furthermore, all previous VO_x nanotube syntheses[17,18] report a dependence on amine alkyl chain length: wider vanadate interlayer spacings resulting from longer intercalated amine alkyl chain lengths. Many of these reports have not, however, clarified the conformation of the amine within the vanadate layer conclusively for all cases. Closing of the innermost vanadate layer predefines the inner diameter, which remains constant throughout the full length of these tubes. Our observations of high yield, thick-walled nanotubes with unprecedented long-range uniformity is encouraging when compared to the current state-of-the-art of concentric closed-centered VO_x nanotubes that have a typical synthesis yield of 1% of such tubes and have been only observed comprising four vanadate layers or less.

Evidence for VO_x layer branching can be seen at **S** and **T** in Fig. 2B. This image highlights the first observation of triplet layers, a feature never before observed.[11,16] The tubes are composed of scrolled layers of vanadate and such near-perfect walls typically have a number density of atomic layers that is a multiple of three; the thickest NT walls observed contain 15 vanadate layers, inferred from the diffraction contrast in multiple TEM images.

The structure of the nanotube in Fig. 2B has a distorted wall with a hole enclosed by the VO_x layers. The contrast of the outer VO_x layers is different at this site; it seems to be divided into two layers which appear with less dark contrast. This can be explained by observing the presence of split VO_x layers, or half-spacings, through the section of the tube. Discrimination is difficult in this projection direction. However, a defect of the latter type (dislocation) is definitely present in tubes in the nanourchin such as that shown in Fig. 3A, where both lattice-plane-inclusion and lattice-plane-termination dislocations are observed at **R**, **S**, **G**, and **H**; a detailed example is shown in the inset. The inset electron diffraction pattern confirms the lattice spacing of 2.85 nm determined from the diffraction spots at **U** and we also observe the presence of weaker intensity half spacing diffraction spots at **V**. This is also observed in a single nanotube (compare **E** and **F** in Fig. 3A) suggesting a scrolling of the layers occurs towards the center of the tube, an observation only partially demonstrated by previous investigations.[12,13,16]

Frequently, tubes in the nanourchin are grown together as indicated by the formation of bundles, i.e., a spherical structure containing radially oriented nanotubes.[13] We also observe that some tubes are connected in an intimate way and appear to share one or more VO_x layers in the form of wall sintering or zipping, forming larger diameter NTs, shown in Fig. 3B-3D. In such cases, only a single hollow center, seen at **X**, is observed along the length of zipped tubes. The zipping occurs with near-perfect lattice plane mixing, where at **L** no dislocations, bending, stacking faults, or half-spacings are observed at the merge point. We also observe evidence of different growth rates of the VO_x layers forming the scrolled walls at **Y** and **Z** with the concomitant lattice-plane-inclusion dislocation forming a bending imperfection in the outer tube wall. Such NTs, however, tend to contain various lattice-plane dislocations similar to those shown at **R** and **S** in Fig. 3A, and seen in more detail in the inset image.

The X-ray diffraction (XRD) analysis of the product after hydrothermal treatment, shown in Fig. 4, shows that the reaction leads to specific crystalline products; the $\{00l\}$ Bragg reflections indicate a lamellar intercalated product of the amine and the vanadium oxide. The peak with the highest intensity is located at a d value of 2.9 nm corroborating the interlayer distance (2.85 nm) as determined by electron diffraction measurements (Fig. 3A). The characteristic $\{hk0\}$ reflections, indexed on the basis of a two-dimensional square lattice with $a = 0.611$ nm, indicate high structural order of both the vanadate layers, but also for the intercalated amine groups between

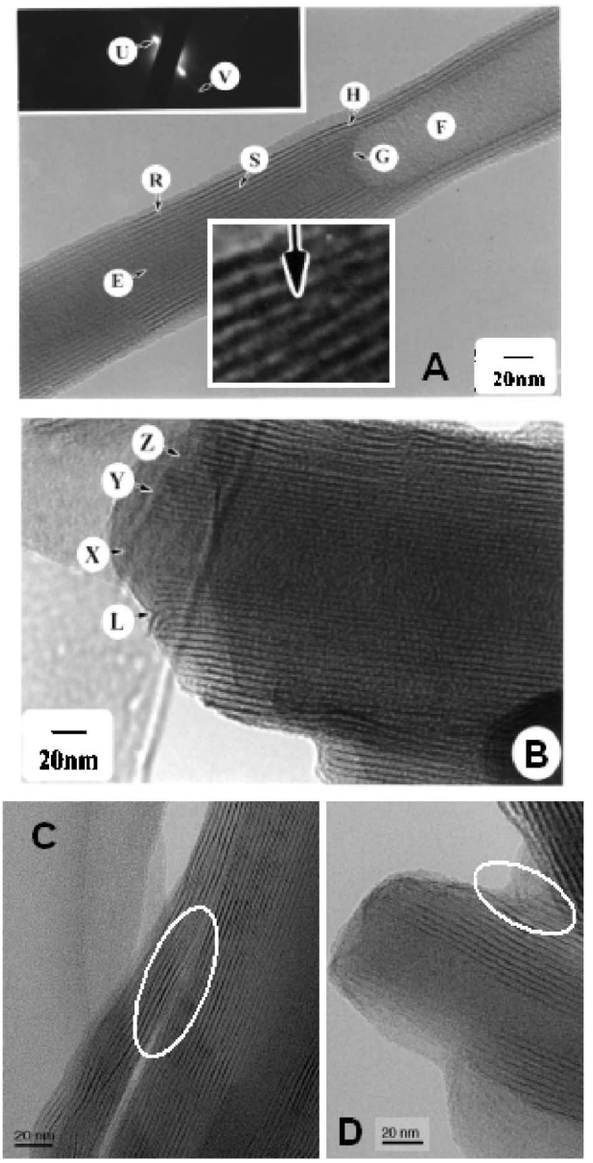

Figure 3. HRTEM images of (A) fully developed nanotube, (inset) selected area electron diffraction pattern of a single tube and high resolution image of a lattice plane dislocation, (B) atomic layer zipping in adjacent nanotube tips forming a large diameter NT (C), (D) adjacent NTs showing areas of atomic layer zipping.

these layers, i.e., these peaks appear at the same 2Θ values even when we employed longer or shorter chained amines as the structural template. The degree of crystallinity is impressive considering that during data acquisition, the nanotubes are oriented in a radial array on the nanourchin structure. The amine chain length did proportionately affect the $\{00l\}$ peaks, however. The measured vanadate interlaminar distance is larger than the amine molecular length ($\sim$2.12 nm) suggesting a double layer of the amine in a *trans* configuration[19] oriented either perpendicularly to the VO_x planes with interpenetrated alkyl chains or forming an angle with them.[11,12,16,20] To estimate the maximum quantity of intercalated surfactant and how it is arranged between the vanadium oxide layers, we employ a simplified version of the model presented by Golub et al.[21] The model allows a comparative analysis of the interlamellar distance of the host-guest nanocomposite determined by XRD together with the geometrical dimensions of the guest (amine).

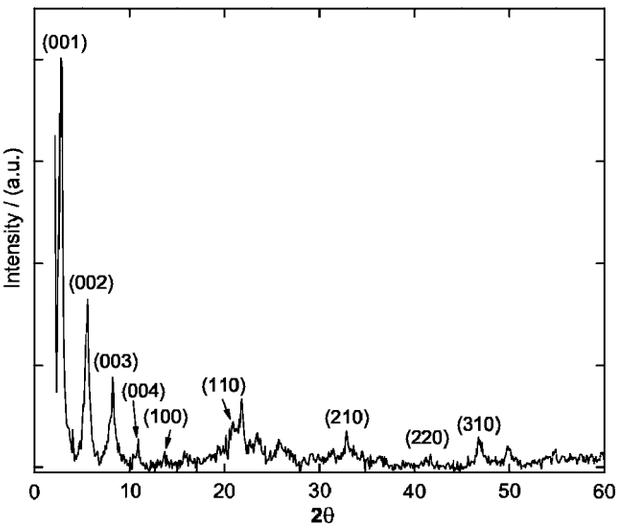

Figure 4. X-ray diffraction analysis of the nanocomposite containing VOTPP and HDA after hydrothermal treatment.

The dimensions of the amine molecule were calculated[22] taking into consideration the van der Waals ratio of the different atoms and the cylindrical volume for the amine. In our system, the length of the HDA molecule, l_{HDA}, is 2.4 nm.

As observed in the powder diffraction pattern in Fig. 4, the hydrothermal treatment of the reaction mixture leads to the formation of a crystalline mesophase formed by lamellar species with interlaminar distances of $\sim$3 nm. The value of the interlaminar distance determined by XRD, d_{XRD}, is thus expressed as the following

$$d_{XRD} = l_{HDA} + \theta_{VO_x} + (\%_{OL} \times l_{HDA}) + T_{(VO_x)}$$

where θ_{VO_x} is the angle that the amine alkyl chain subtends to the normal within the VO_x lamina, $\%_{OL}$ is the percentage overlap of the amine alkyl chains and $T_{(VO_x)}$ is the thickness of a single vanadate lamina (0.28 nm). Thus, we estimate this distance to be similar to a monolayer arrangement of hexadecylamine chains alternatively oriented in opposite directions within the tube walls, with a bilayer of chains in the all-*trans* conformation with a 10–30% overlap between neighboring chains for angles of 0–30° to the normal within the vanadate interlayer spacing. A van der Waals interaction is assumed to realize its uniform and periodic, albeit wide, 2.85 nm dimension.

In Fig. 5, we observe atomic layer zipping of adjacent tubes as opposed to coalescence observed in CNTs.[23] Previous work[24] on vanadate nanotubes has shown that the residual-organic template is destroyed at high temperature while the wall structure was maintained, although no agglomerated or sinterized tubes were observed. Unlike previous attempts,[17] cross-sectional and plan view HRTEM observations did not result in any morphological change, blurring of the associated electron diffraction reflections, nor contrast reduction in images.

A previously reported mechanism[11] suggests a bending of an intermediate composite with a lamellar arrangement of parallel VO_x layers separated by the synthesis template followed by closure of the layers during NT formation. However, this only partially explains the observed wall structures and their dependence on the number of vanadate layers.

Conclusions

In summary, nanotubes in the nanourchin do not tend to consist solely of coaxial cylinders or scrolled layers but an ordered mixture of both. The tubes have a multi-walled structure, composed of sheets of scrolled vanadium oxide layers. We also demonstrate the overlapping of triplet-vanadate-layer scrolls in the NTs, seen in Fig. 5A,

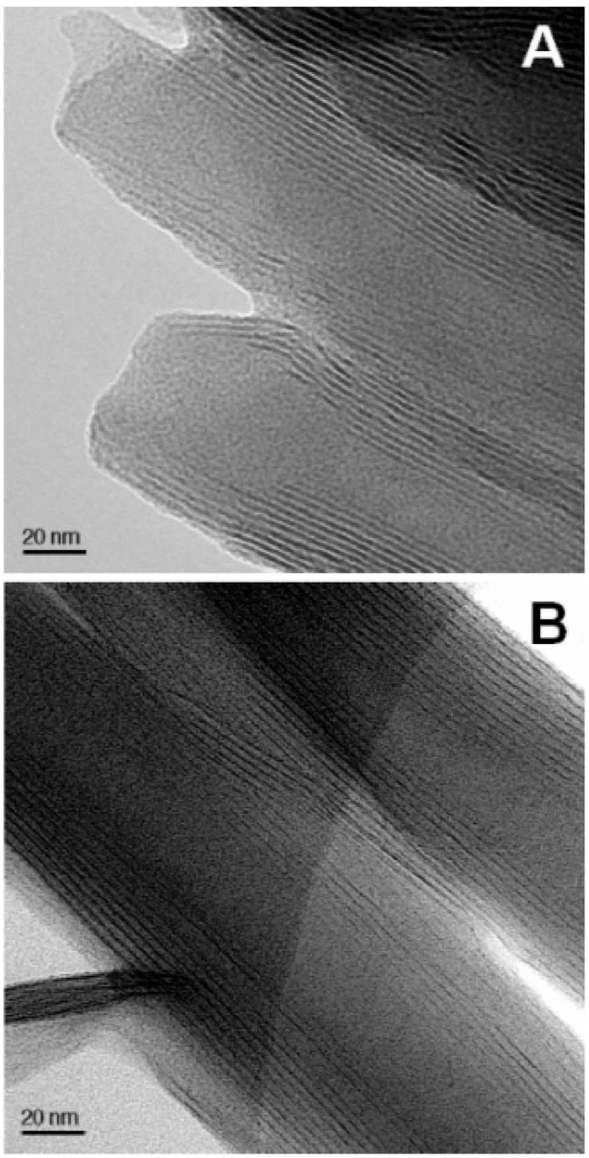

Figure 5. High-resolution bright field TEM image along (A) direct and (B) angled longitudinal directions showing the nanotube cross sections.

although it tends to be most obvious in the more defective, thinner walled nanotubes. Current efforts are focused on explaining the driving force behind layer bending and rolling in order to understand the necessary conditions for defect free synthetic methods of VO_x-NT formation and in the determination of the chirality of agglomerated tubes in the nanourchin. Such structural information is critical in determining the suitability of these materials for ion-intercalated rechargeable battery technologies. The amine can be substituted by various metal cations, via proton exchange with neutral diamines or even thiols for metal nanoparticle incorporation.[25]

Acknowledgments

This material is based upon work supported by the Science Foundation Ireland under grant no. 02/IN.1/172. Support from FONDECyT (grants 1050344, 1030102, 7050081), the University of Chile, and the Universidad Tecnológica Metropolitana are also gratefully acknowledged.

Tyndall National Institute assisted in meeting the publication costs of this article.

References

1. Y. Huang, X. Duan, Q. Wei, and C. M. Leiber, *Science*, **291**, 630 (2001).
2. A. P. Alivisatos, *Science*, **271**, 933 (1996).
3. Y. Sun and Y. Xia, *Science*, **298**, 2176 (2002).
4. D. Yu and W. V. Yam, *J. Am. Chem. Soc.*, **126**, 1320 (2004).
5. S. K. Chung, N. A. Cimilenko, A. Y. Borovykov, and S. H. Lee, *J. Power Sources*, **84**, 6 (1999).
6. E. Shembel, R. Apostolova, V. Nagirny, D. Aurbach, and B. Markovsky, *J. Power Sources*, **81–82**, 480 (1999).
7. D. B. Lee, S. Passerini, A. L. Tipton, B. B. Owens, and W. H. Smyrl, *J. Electrochem. Soc.*, **142**, L102 (1995).
8. S. Nordlinder, K. Edström, and T. Gustafsson, *Electrochem. Solid-State Lett.*, **4**, A129 (2001).
9. M. Winter, J. O. Besenhard, M. E. Spahr, and P. Novák, *Adv. Mater. (Weinheim, Ger.)*, **10**, 725 (1998).
10. J. M. Reinoso, H.-J. Muhr, M. Niederberger, F. Bieri, B. Schnyder, and R. Nesper, *Helv. Chim. Acta*, **83**, 1724 (2000).
11. R. Nesper and H.-J. Muhr, *Chimia*, **52**, 571 (1998).
12. G. R. Patzke, F. Krumeich, and R. Nesper, *Angew. Chem., Int. Ed.*, **41**, 2446 (2002).
13. C. O'Dwyer, D. Navas, V. Lavayen, E. Benavente, M. A. Santa Ana, G. González, S. B. Newcomb, and C. M. Sotomayor Torres, *Chem. Mater.*, **18**, 3016 (2006).
14. V. Lavayen, C. O'Dwyer, S. B. Newcomb, M. A. Santa Ana, E. Benavente, G. González, and C. M. Sotomayor Torres, *Phys. Status Solidi B*, **243**, 3285 (2006).
15. C. O'Dwyer, V. Lavayen, M. A. Santa Ana, S. B. Newcomb, E. Benavente, G. González, and C. M. Sotomayor Torres, *Chem. Mater.*, In press.
16. X. Chen, X. Sun, and Y. Li, *Inorg. Chem.*, **41**, 4524 (2002).
17. F. Krumeich, H.-J. Muhr, M. Niederberger, F. Bieri, B. Schnyder, and R. Nesper, *J. Am. Chem. Soc.*, **121**, 8324 (1999).
18. H.-J. Muhr, F. Krumeich, U. P. Schönholzer, F. Bieri, M. Niederberger, L. J. Gauckler, and R. Nesper, *Adv. Mater. (Weinheim, Ger.)*, **12**, 231 (2000).
19. L. Peng, J. Yu, J. Li, Y. Li, and R. Xu, *Chem. Mater.*, **17**, 2101 (2005).
20. V. Lavayen, M. A. Santa Ana, G. González, J. Seekamp, and C. M. Sotomayor Torres, *Mol. Cryst. Liq. Cryst.*, **416**, 49 (2004).
21. A. S. Golub, I. B. Shumilova, Y. N. Novikov, J. L. Mansot, and M. Danot, *Solid State Ionics*, **91**, 307 (1996).
22. Hyperchem v5.01, Hypercube Inc., Waterloo, Ontario, Canada.
23. M. Terrones, H. Terrones, F. Banhart, J.-C. Charlier, and P. M. Ajayan, *Science*, **288**, 1226 (2000).
24. W. Chen, L. Mai, J. Peng, X. Qing, and Q. J. Zhu, *Solid State Chem.*, **177**, 377 (2004).
25. V. Lavayen, C. O'Dwyer, G. González, G. Cárdenas, and C. M. Sotomayor Torres, *Mater. Res. Bull.*, doi: 10.1016/j.materresbull.2006.07.022.